Scottish Universities Environmental Research Centre

# OSL investigations at Hardisty, Alberta, Canada

## Sections HD03, HD04 & HD05

August 2015

T.C. Kinnaird[1], K. Munyikwa[2] and D.C.W. Sanderson[1]

[1]SUERC, East Kilbride, Scotland, UK
[2]Athabasca University, 1 University Drive, Athabasca, Alberta, T8N 1T3, Canada

**East Kilbride Glasgow G75 0QF Telephone: 01355 223332 Fax: 01355 229898**

**Preface.** This is the second in a series of two reports which describe the luminescence dating methods used to construct chronologies for sediment stratigraphies associated with, and enclosing artefacts of First Nations historic significance in the Battle River Valley area, near Hardisty, east-central Alberta. The luminescence ages reported herein, and in the previous report, provide the chronological control to the archaeological investigations at this site, led by Rob Wondrasek, and commissioned by Enbridge, ahead of the construction of the Edmonton-Hardisty Pipeline.

The background to the luminescence investigations is provided in the previous report:

> 'Kinnaird, T.C., Munyikwa, K. and Sanderson, D.C.W. January 2015. OSL investigations at Hardisty, Alberta, Canada. SUERC dating report, SUERC, p. 1-21.' http://eprints.gla.ac.uk/110540/

The results of the 2014 dating programme are re-tabulated here, as the luminescence ages are from sedimentary sequences which directly relate to those sampled in January 2015.

**Summary**
This report is concerned with optically stimulated luminescence (OSL) investigations of a number of sediment stratigraphies in the Battle River Valley area, near Hardisty, east-central Alberta. Archaeological investigations in this region, led by Rob Wondrasek, have identified thousands of historical artefacts, including projectile points and lithic fragments indicative of occupation. Ken Munyikwa visited the archaeological sites at Hardisty in June 2014 and January 2015 to sample key units within the sediment stratigraphies for OSL dating. The sediments associated with the artefacts were appraised through five profiles, Hardisty-1 (HD01) to Hardisty-5 (HD05), comprised of 43 field-profiling and 14 dating samples. Profiles HD01 and HD02 were sampled in June 2014; and profiles HD03 through to HD05 in January 2015. The dating questions associated with these materials relate to the age of artefact-bearing horizon, through dating the enclosing sediments above and beneath the archaeological soil, it should be possible to provide terminus post quem (TPQ) and terminus ante quem (TAQ) on the age of the artefacts.

The conventional quartz SAR OSL approach was examined as a potential method for providing the depositional ages of the sediment enclosing the artefacts. Luminescence profiling during fieldwork had revealed stratigraphically progressive IRSL and OSL signals, indicating sediment with dating potential. Dose rate estimates from these sediments were assessed using a combination of high resolution gamma spectrometry (HRGS) and thick source beta counting (TSBC), reconciled with each other, water contents and modelled micro-dosimetry. Where appropriate, the external gamma dose rates received at the position of the dating sample were reconstructed from the adjacent bulk gamma spectrometry samples, yielding wet gamma dose rates between 0.42 and 0.54 mGy $a^{-1}$, which are comparable with those recorded at each sampling position.

Equivalent doses were determined by OSL from 16-48 aliquots of quartz per sample (depending on quartz yields) using a single-aliquot-regenerative (SAR) approach. The material exhibited good OSL sensitivity and produced acceptable SAR internal quality control performance. Radial plotting methods revealed some heterogeneity in the equivalent dose distributions of each sample, indicating that each sample enclosed mixed-age materials, reflecting variable bleaching at deposition. The field profiles provide some measure of control on this. Luminescence ages were calculated using standard microdosimetric models, with uncertainties that combined measurement and fitting errors from the SAR analysis, all dose rate evaluation uncertainties, and allowance for the calibration uncertainties of the sources and reference materials.

The quartz OSL ages reported here for the sand sequences at HD03 to HD05, contribute to the expanding catalogue of chronological data on the depositional sequences at Hardisty, and further, provide the means to assess the temporal and spatial distribution of artefacts across the site. The sediment chronologies established for each profile are internally and mutually coherent, spanning at HD03 from 7.3 ± 0.3 ka (SUTL2778) to 9.0 ± 0.5 ka (SUTL2780), at HD04 from 7.0 ± 0.3 ka (SUTL2781) to 8.3 ± 0.4 ka (SUTL2782), and at HD05 from 8.3 ± 0.5 ka (SUTL2783) to 9.6 ± 0.6 ka (SUTL2785). The field profile at HD05 reveals some complexity to its depositional history, with notable maxima and inversions in intensities from 150cm depth, potentially reflecting reworking and re-deposition of sediment within this sequence. TAQ for this phase of reworking is provided by the youngest unit examined in the profile, which at 7.5 ± 0.6 ka (SUTL2784), is consistent with the occupational phase recorded in the adjacent sections. The

sediment chronologies established in this dating campaign, and in the 2014 campaign, are synchronous suggesting contemporaneous deposition across the site, and presumably, with local knowledge, scope for further age modelling including the use of Bayesian methods to refine the TAQ and TPQ age limits.

**Contents**

**List of figures**



**List of tables**

## 1. Introduction

This report is concerned with optically stimulated luminescence (OSL) investigations of sediment from the Hardisty archaeological sites, approximately 2 km SW of Hardisty, east central Alberta (Canada). Enbridge commissioned the archaeological investigations ahead of the development of Enbridge Edmonton to Hardisty Pipeline Project - the construction of a 36-inch diameter crude oil pipeline linking terminals in Edmonton and Hardisty. Excavation work for the project discovered archaeological artefacts in the pipeline's right-of-way at a site near Hardisty (Fig. 1-1). The artefacts comprised thousands of historical artefacts of First Nations significance, including projectile points and lithic fragments indicative of occupation. The OSL investigations form one part of a historic resources impact assessment study that is being carried out to characterize the archaeological site. The study also aims to evaluate the impact of the pipeline related excavations and to advise on any mitigative measures that may be considered necessary to minimise any deleterious effects.

The objective of the OSL investigation is to provide chronological control for the geo-archaeological and stratigraphic investigations of key sedimentary sequences examined at Hardisty. It generates detailed chronological framework for five profiles - Hardisty-01 (HD01), Hardisty-02 (HD02), Hardisty-03 (HD03), Hardisty-04 (HD04) and Hardisty-05 (HD05). Profiles HD01 and HD02 were sampled in June 2014 (Kinnaird etal. 2015); and profiles HD03 through to HD05 in January 2015. Samples collected for analysis comprised 43 field-profiling and 14 dating samples. The dating questions associated with these materials relate to the age of the artefact-bearing horizon. By dating the enclosing sediments collected from above (5 samples) and beneath (4), as well as within the archaeological soil (5), it should be possible to provide terminus post quem (TPQ) and terminus ante quem (TAQ) on the age of the artefacts.

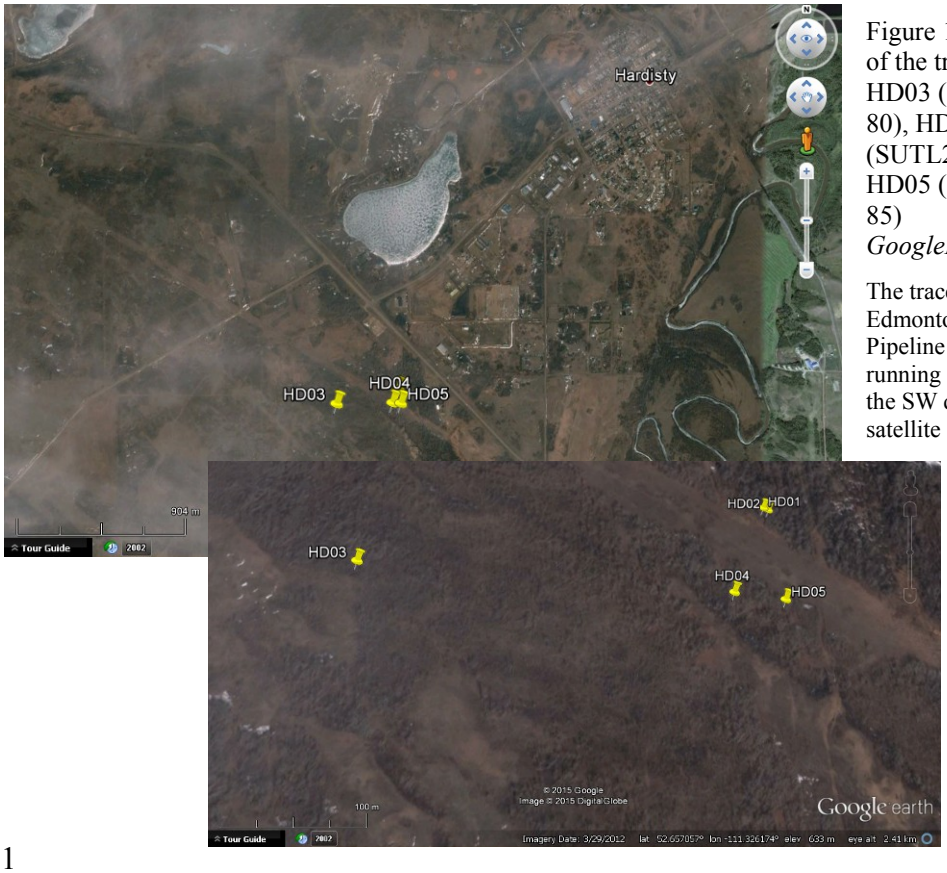


Figure 1-1: Location of the trenches at HD03 (SUTL2778-80), HD04 (SUTL2781-82) and HD05 (SUTL2783-85) *GoogleEarth image*

The trace of the Edmonton to Hardisty Pipeline is observed running c. WNW-ESE in the SW quadrant of the satellite image

## 2. Sampling

Sampling was undertaken by Ken Munyikwa in June 2014 and January 2015. The five investigated sections, are all within 400 m of one another and occur on a rolling sandy landscape, thought to be aeolian in origin. At depth, the sands enclose multiple projectile points and lithic fragments indicative of human occupation. In each section, samples were taken from the units above and beneath the artefact-bearing horizon, as well as within the unit enclosing the finds.

In section HD-01, sands were sampled at depths of 175, 197 and 213 cm, enclosing the artefact-bearing horizon between 187 and 207 cm. At the time of sampling (June 2014), the uppermost sample was taken just above the current water table (at c. 190 cm), whereas the lower samples were taken from beneath the water table. In section HD-02, the sand units were sampled at depths of 164, 179 and 194 cm, with the artefact bearing horizon between 169 and 189 cm. As in HD-01, the uppermost sample was taken just above the water table (at c. 175 cm), and the lower two samples beneath the water table. In section HD-03 (Fig. 2-1a), sands were sampled at depths of 141, 156 and 176 cm; in section HD-04 (Fig. 2-1b),, at depths of 140 and 160 cm; and in section HD-05 (Fig. 2-1c),, at depths of 143, 163, and 183 cm.

The sandy deposits at the investigated sites are fine-grained and well-drained. Hence, it is expected that water would drain through the sediment freely. Hardisty is in the Prairie Ecozone, with annual precipitation around 400 mm (semiarid), highest in June/July/August. In Spring, snow melt and ground thaw may lead to temporary saturation at lower levels, usually complete within a month. Therefore, the samples at lower levels (below c. 1.8 m) might be expected to be below the water table for a maximum of 3 months a year, and one can assume similar conditions throughout the burial history of the samples. There may be temporary fluctuations upwards with episodes of high precipitation but because of the good drainage, these are not long lasting. This observation, coupled with laboratory determinations of the received and saturated water contents of the dating samples, was used to elucidate on the water contents for use in dose rate determination (see section 3.1.1.).

The samples were submitted for dating at the SUERC luminescence laboratories in two batches in August 2014 (HD01 and HD02, Kinnaird etal. 2015) and March 2015 (HD03 through to HD05). A brief description of the samples is given in Table 2-1, together with the laboratory (SUTL) numbers assigned to each sample on arrival at the SUERC luminescence laboratories. Photographs of the sections (Figs 2-1 to 2-3), together with luminescence profiling data obtained using portable OSL instrumentation (Figs 2-1 to 2-3) were provided. Initial luminescence screening was undertaken by Ken Munyikwa to characterise the luminescence properties of the sediments surrounding the units sampled for dating (Table 2-1; Figs 2-1 to 2-3). In profiles HD03 and HD04, IRSL and OSL signal intensities increase down section, consistent with a normal age-depth progression, and suggesting favourable behaviour for luminescence dating. In contrast, profile HD05, revealed a more complex depositional history, with the lower part of the profile characterised by inversions and maxima in IRSL and OSL signal intensities (from c. 150 cm depth), consistent with reworking and re-deposition of the lower layers.

| Location | Field no. | SUTL no. | Depth /cm | Context | Archaeological significance |
|---|---|---|---|---|---|
| Hardisty 03 | ***52°N 39.474', 111°W 19.835'*** | | | | |
| | OSL1 | 2778 | 141 | sand unit (possibly aeolian), overlying a human occupation level that contains multiple projectile points (thought to be of mid-Hocene age) | provides TAQ for the age of the human occupation level |
| | OSL2 | 2779 | 156 | sand unit (possibly aeolian), containing multiple projectile points | provides constraint on the age of the human occupation level |
| | OSL3 | 2780 | 176 | base of sand unit (possibly aeolian), containing multiple projectile points | provides TPQ for the age of the human occupation level |
| Hardisty 04 | ***52° 39.472'N, 111° 19.553'W*** | | | | |
| | OSL1 | 2781 | 140 | sand unit (possibly aeolian), overlying a human occupation level that contains multiple projectile points (thought to be of mid-Hocene age) | provides TAQ for the age of the human occupation level |
| | OSL2 | 2782 | 160 | sand unit (possibly aeolian), containing multiple projectile points | provides constraint on the age of the human occupation level |
| Hardisty 05 | ***52° 39.470'N, 111° 19.511'W*** | | | | |
| | OSL1 | 2783 | 143 | sand unit (possibly aeolian), overlying a human occupation level that contains multiple projectile points (thought to be of mid-Hocene age) | provides TAQ for the age of the human occupation level |
| | OSL2 | 2784 | 163 | sand unit (possibly aeolian), containing multiple projectile points | provides constraint on the age of the human occupation level |
| | OSL3 | 2785 | 183 | base of sand unit (possibly aeolian), containing multiple projectile points | provides TPQ for the age of the human occupation level |
| Hardisty 01 | ***52° 39.520'N, 111° 19.520'W*** | | | | |
| | OSL1 | 2692 | 175 | sand unit (possibly aeolian), overlies strata enclosing multiple projectile points (potentially early to mid-Holocene); | provides TAQ for artefact-bearing horizon |
| | OSL2 | 2693 | 197 | sand unit (possibly aeolian), contains multiple projectile points and lithic fragments indicative of human occupation | provides constraint on the age of the human occupation level |
| | OSL3 | 2694 | 213 | sand unit (possibly aeolian), underlies strata enclosing multiple projectile points | provides TPQ for artefact-bearing horizon |
| Hardisty 02 | ***52° 39.519'N, 111° 19.516'W*** | | | | |
| | OSL1 | 2695 | 164 | sand unit (possibly aeolian), overlies strata enclosing multiple projectile points (potentially early to mid-Holocene); | provides TAQ for artefact-bearing horizon |
| | OSL2 | 2696 | 179 | sand unit (possibly aeolian), contains multiple projectile points and lithic fragments indicative of human occupation | provides constraint on the age of the human occupation level |
| | OSL3 | 2697 | 194 | sand unit (possibly aeolian), underlies strata enclosing multiple projectile points | provides TPQ for artefact-bearing horizon |

Table 2-1: Sample descriptions, contexts and archaeological significance of SUTL2692-2697 and SUTL2778-2785

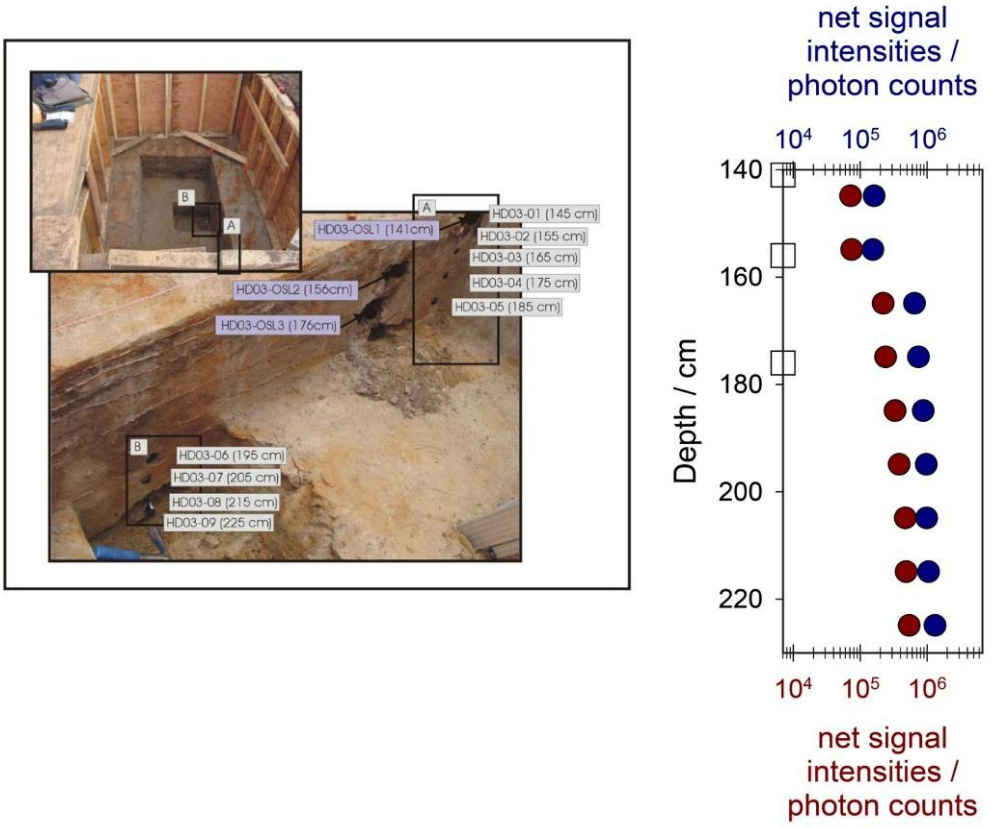


Figure 2-1: a) Photographs of the sediment stratigraphy at HD03, b) luminescence signal intensities plotted vs depth for the same sediment profile

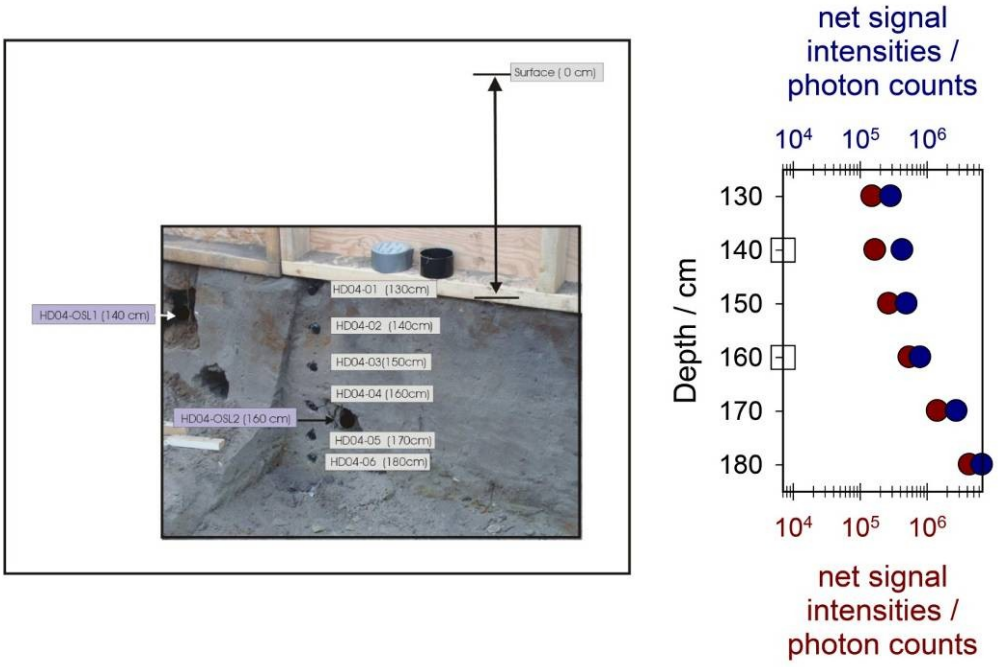


Figure 2-2: a) Photographs of the sediment stratigraphy at HD04, b) luminescence signal intensities plotted vs depth for the same sediment profile

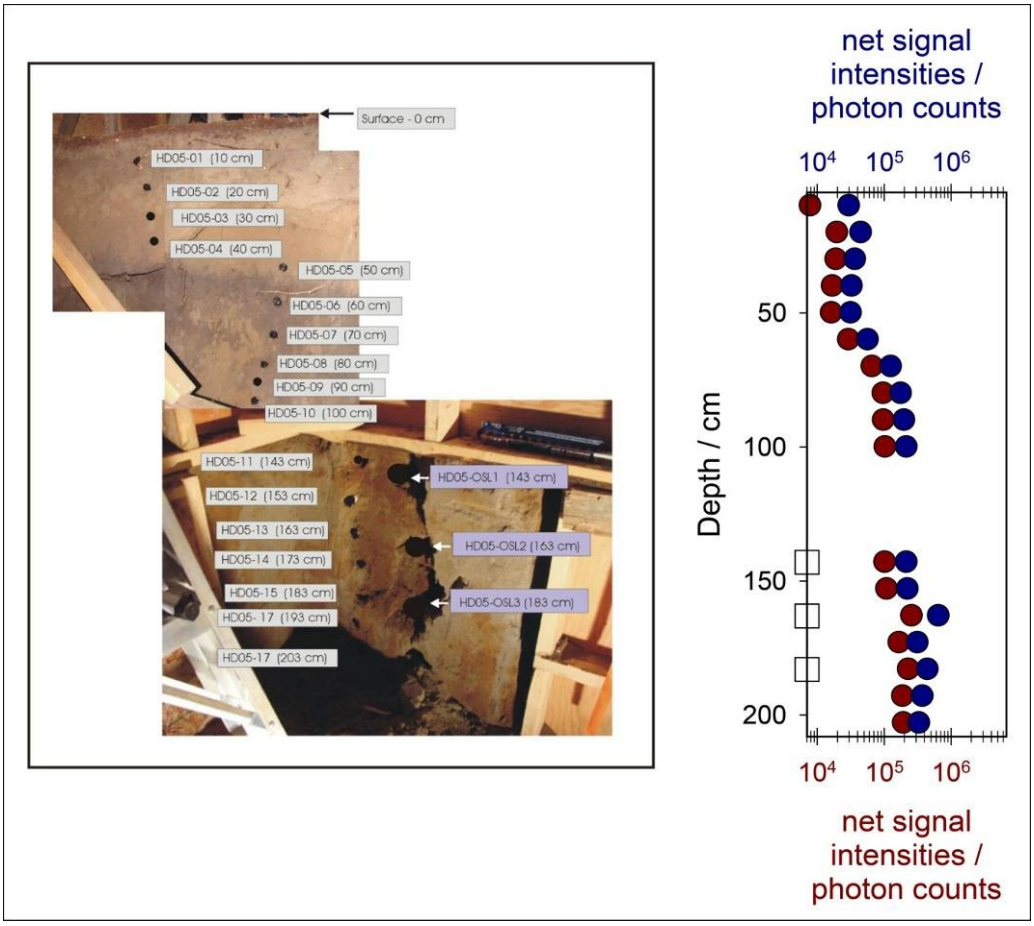


Figure 2-3: a) Photographs of the sediment stratigraphy at HD05, b) luminescence signal intensities plotted vs depth for the same sediment profile

# 3. Quartz SAR measurements

## 3.1. Sample preparation

All sample handling and preparation was conducted under safelight conditions in the SUERC luminescence dating laboratories.

### 3.1.1. Water contents

Bulk samples were weighed, saturated with water and re-weighed. Following oven drying at 50 °C to constant weight, the actual and saturated water contents were determined as fractions of dry weight. These data were used, together with information on field conditions to determine water contents and an associated water content uncertainty for use in dose rate determination.

### 3.1.2. HRGS and TSBC Sample Preparation

Bulk quantities of material, weighing c. 50g, were removed from each full dating sample for environmental dose rate determinations. This material was placed in an oven to dry to constant weight. Approximately 50g quantities of dried material from

each sample were weighed into high-density-polyethylene (HDPE) pots for a high-resolution gamma spectrometry (HRGS) measurement. Each pot was sealed with epoxy resin and left for 3 weeks prior to measurement to allow equilibration of $^{222}$Rn daughters. Sub-quantities of 20 g of the dried material was used in thick source beta counting (TSBC; Sanderson, 1988).

#### 3.1.3. Quartz mineral preparation

Approximately 20g of material was removed for each tube and processed to obtain sand-sized quartz grains for luminescence measurements. Each sample was wet sieved to obtain the 90-150 and 150-250 μm fractions. The 150-250 μm sub-sample was treated with 1 M hydrochloric acid (HCl) for 10 minutes, 15% hydrofluoric acid (HF) for 15 minutes, and 1 M HCl for a further 10 minutes. The HF-etched sub-samples were then centrifuged in sodium polytungstate solutions of ~2.51, 2.58, 2.62, and 2.74 gcm$^{-3}$, to obtain concentrates of potassium-rich feldspars (2.51-2.58 gcm$^{-3}$), sodium feldspars (2.58-2.62 gcm$^{-3}$) and quartz plus plagioclase (2.62-2.74 gcm$^{-3}$). The selected quartz fraction was then subjected to further HF and HCl washes (40% HF for 10mins, followed by 1M HCl for 10 mins). All materials were dried at 50°C and transferred to Eppendorf tubes. The 40%HF-etched, 2.62-2.74 gcm$^{-3}$ 'quartz' fractions were dispensed to 10mm stainless steel discs for measurement. 16-48 aliquots were produced for each sample (depending on quartz yields).

### 3.2. Measurements and determinations

#### 3.2.1. Dose rate determinations

Dose rates were measured in the laboratory using HRGS and TSBC. Full sets of laboratory dose rate determinations were made for all samples.

HRGS measurements were performed using a 50% relative efficiency "n" type hyper-pure Ge detector (EG&G Ortec Gamma-X) operated in a low background lead shield with a copper liner. Gamma ray spectra were recorded over the 30 keV to 3 MeV range from each sample, interleaved with background measurements and measurements from SUERC Shap Granite standard in the same geometries. Sample counts were for 80ks. The spectra were analysed to determine count rates from the major line emissions from $^{40}$K (1461 keV), and from selected nuclides in the U decay series ($^{234}$Th, $^{226}$Ra + $^{235}$U, $^{214}$Pb, $^{214}$Bi and $^{210}$Pb) and the Th decay series ($^{228}$Ac, $^{212}$Pb, $^{208}$Tl) and their statistical counting uncertainties. Net rates and activity concentrations for each of these nuclides were determined relative to Shap Granite by weighted combination of the individual lines for each nuclide. The internal consistency of nuclide specific estimates for U and Th decay series nuclides was assessed relative to measurement precision, and weighted combinations used to estimate mean activity concentrations (Bq kg$^{-1}$) and elemental concentrations (% K and ppm U, Th) for the parent activity. These data were used to determine infinite matrix dose rates for alpha, beta and gamma radiation.

Beta dose rates were also measured directly using the SUERC TSBC system (Sanderson, 1988). Count rates were determined with six replicate 600 s counts on each sample, bracketed by background measurements and sensitivity determinations using the Shap Granite secondary reference material. Infinite-matrix dose rates were calculated by scaling the net count rates of samples and reference material to the working beta dose rate of the Shap Granite (6.25 ± 0.03 mGy a$^{-1}$). The estimated

errors combine counting statistics, observed variance and the uncertainty on the reference value.

The dose rate measurements were used in combination with the assumed burial water contents, to determine the overall effective dose rates for age estimation. Cosmic dose rates were evaluated by combining latitude and altitude specific dose rates (0.19 ± 0.01 mGy $a^{-1}$) for the site with corrections for estimated depth of overburden using the method of Prescott and Hutton (1994).

### 3.2.2. Quartz SAR luminescence measurements

All measurements were conducted using a Risø DA-15 automatic reader equipped with a $^{90}Sr/^{90}Y$ β-source for irradiation, blue LEDs emitting around 470 nm and infrared (laser) diodes emitting around 830 nm for optical stimulation, and a U340 detection filter pack to detect in the region 270-380 nm, while cutting out stimulating light (Bøtter-Jensen et al., 2000). For each sample, equivalent dose determinations were made on sets 16-48 aliquots per sample, using a single aliquot regeneration (SAR) sequence (cf Murray and Wintle, 2000). According to this procedure, the OSL signal level from an individual disc is calibrated to provide an absorbed dose estimate (the equivalent dose) using an interpolated dose-response curve, constructed by regenerating OSL signals by beta irradiation in the laboratory. To assess the dependence of equivalent dose on preheat, and the thermal stability of the OSL signal, eight different preheat temperatures were investigated (200 to 260°C, in 10°C increments, then 280°C). Sensitivity changes which may occur as a result of readout, irradiation and preheating (to remove unstable radiation-induced signals) are monitored using small test doses after each regenerative dose. Each measurement is standardised to the test dose response determined immediately after its readout, to compensate for observed changes in sensitivity during the laboratory measurement sequence. For the purposes of interpolation, the regenerative doses are chosen to encompass the likely value of the equivalent (natural) dose. A repeat dose point is included to check the ability of the SAR procedure to correct for laboratory-induced sensitivity changes (the 'recycling test'), a zero dose point is included late in the sequence to check for thermally induced charge transfer during the irradiation and preheating cycle (the 'zero cycle'), and an IR response check is included to assess the magnitude of non-quartz signals. Regenerative dose response curves were constructed using doses of 1, 5, 10 and 30 Gy, with a test dose of 2 Gy. (In the 2014 dating campaign, regenerative doses of 2.5, 5, 10, 50, 0 and 2.5 Gy were used, with a test dose of 2 Gy)

## 3.3. Results

### 3.3.1. Dose rates

HRGS results are shown in Table 3-1, both as activity concentrations (i.e. disintegrations per second per kilogram) and as equivalent parent element concentrations (in % and ppm), based in the case of U and Th on combining nuclide specific data assuming decay series equilibrium. K concentrations ranged from 1.1 to 1.2 %. U concentrations ranged from 0.6 to 1.2 ppm. Th concentrations ranged from 2.2 to 3.6 ppm. Similar equivalent concentrations were obtained by HRGS for the dating samples collected from profiles HD01 and HD02 (Appendix A): K concentrations ranged from 1.1 to 1.3 %; U concentrations ranged from 0.5 to 0.8

ppm; and Th concentrations from 2.3 to 3.4 ppm. This is consistent with similar lithological units being sampled in 2014 and 2015.

| SUTL no. | Activity Concentration[a] / Bq kg$^{-1}$ | | | Equivalent Concentration[b] | | |
|---|---|---|---|---|---|---|
| | K | U | Th | K / % | U / ppm | Th / ppm |
| 2778 | 385 ± 16 | 15 ± 1.3 | 15 ± 1.1 | 1.24 ± 0.05 | 1.22 ± 0.10 | 3.64 ± 0.28 |
| 2779 | 348 ± 16 | 10 ± 1.1 | 11 ± 1.1 | 1.12 ± 0.05 | 0.80 ± 0.09 | 2.67 ± 0.26 |
| 2780 | 362 ± 16 | 10 ± 1.1 | 12 ± 1.1 | 1.17 ± 0.05 | 0.85 ± 0.09 | 2.85 ± 0.26 |
| 2781 | 353 ± 16 | 10 ± 1.1 | 10 ± 1.0 | 1.14 ± 0.05 | 0.79 ± 0.09 | 2.47 ± 0.25 |
| 2782 | 362 ± 16 | 8 ± 1.1 | 11 ± 1.1 | 1.17 ± 0.05 | 0.68 ± 0.09 | 2.70 ± 0.27 |
| 2783 | 357 ± 16 | 7 ± 1.0 | 11 ± 1.0 | 1.15 ± 0.05 | 0.57 ± 0.08 | 2.68 ± 0.26 |
| 2784 | 352 ± 15 | 9 ± 1.1 | 9 ± 1.1 | 1.14 ± 0.05 | 0.74 ± 0.09 | 2.21 ± 0.26 |
| 2785 | 363 ± 16 | 10 ± 1.1 | 9 ± 1.0 | 1.17 ± 0.05 | 0.79 ± 0.09 | 2.21 ± 0.26 |

Table 3-1: Activity and equivalent concentrations of K, U and Th determined by HRGS
[a]Shap granite reference, working values determined by David Sanderson in 1986, based on HRGS relative to CANMET and NBL standards.
[b]Activity and equivalent concentrations for U, Th and K determined by HRGS (Conversion factors based on NEA (2000) decay constants): 40K: 309.3 Bq kg$^{-1}$ %K$^{-1}$, 238U: 12.35 Bq kg$^{-1}$ ppmU$^{-1}$, 232Th: 4.057 Bq kg$^{-1}$ ppm Th$^{-1}$.

Infinite matrix alpha, beta and gamma dose rates from HRGS are listed for all samples in Table 3-2, together with infinite matrix beta dose rates from TSBC. Gamma dose rates measured on the dry samples in the laboratory (HRGS) ranged from 0.5 to 0.6 mGy a$^{-1}$, consistent to those reported previously for the adjacent sections (0.5-0.6 mGy a$^{-1}$; Appendix A). The infinite matrix beta dose rate as determined by HRGS varied between 1.1 and 1.3 mGy a$^{-1}$ (1.1-1.3 mGy a$^{-1}$; Appendix A) and as measured by TSBC between 0.9-1.3 mGy a$^{-1}$ (1.0-1.3 mGy a$^{-1}$; Appendix A).

| SUTL no. | HRGS, dry[a] / mGy a$^{-1}$ | | | TSBC, dry / mGy a$^{-1}$ |
|---|---|---|---|---|
| | Alpha | Beta | Gamma | |
| 2778 | 6.09 ± 0.35 | 1.32 ± 0.05 (3.6%) | 0.63 ± 0.02 (3.6%) | 1.27 ± 0.07 |
| 2779 | 4.20 ± 0.31 | 1.13 ± 0.04 (3.9%) | 0.50 ± 0.02 (4.2%) | 1.11 ± 0.06 |
| 2780 | 4.46 ± 0.32 | 1.18 ± 0.05 (3.8%) | 0.53 ± 0.02 (4.0%) | 1.09 ± 0.06 |
| 2781 | 4.01 ± 0.30 | 1.13 ± 0.04 (3.9%) | 0.49 ± 0.02 (4.1%) | 1.13 ± 0.05 |
| 2782 | 3.88 ± 0.32 | 1.15 ± 0.05 (4.0%) | 0.50 ± 0.02 (4.3%) | 1.04 ± 0.06 |
| 2783 | 3.56 ± 0.3 | 1.12 ± 0.04 (4.0%) | 0.48 ± 0.02 (4.2%) | 0.93 ± 0.06 |
| 2784 | 3.69 ± 0.32 | 1.12 ± 0.04 (3.9%) | 0.47 ± 0.02 (4.4%) | 0.94 ± 0.07 |
| 2785 | 3.82 ± 0.31 | 1.15 ± 0.04 (3.9%) | 0.49 ± 0.02 (4.3%) | 0.88 ± 0.06 |

Table 3-2: Infinite matrix dose rates determined by HRGS and TSBC.
[a]based on dose rate conversion factors in Aikten (1983) and Sanderson (1987)

The water content measurements with assumed values for the average water content during burial are given in Table 3-3. The table also lists the gamma dose rate from the HRGS after application of a water content correction. Effective dose rates to the HF etched 200 μm quartz grains are given for the gamma dose rate and beta dose rate (the mean of the TSBC and HRGS data, accounting for water content and grain size). Field (ranging from 3 to 8% of dry weight) and saturated (12 to 21% of dry weight) water contents were determined from all samples in the laboratory (Table 3-3), with working values between 11 - 14 ± 8% adopted for effective dose rate evaluation. Effective beta dose rates ranged between 0.8 and 1.1 mGy a$^{-1}$ (similar to those

obtained from the adjacent stratigraphies, 0.8-0.9 mGy $a^{-1}$; Appendix A), and the effective gamma dose rates between 0.4 and 0.6 mGy $a^{-1}$ (0.4 mGy $a^{-1}$; Appendix A). For the HD03 and HD05 sections, the external gamma dose rates as received at the position of each dating sample was reconciled with the two adjacent bulk gamma spectrometry samples (Table 3-4), using a distance weighted mean.

The total effective dose rates ranged between 1.5 and 1.7 mGy $a^{-1}$ for the samples collected from section HD-03, between 1.4 and 1.5 mGy $a^{-1}$ for section HD-04, and were consistently around 1.4 mGy $a^{-1}$ for section HD-05.

| SUTL | Water content / % | | | Effective Dose Rate / mGy $a^{-1}$ | | | |
|---|---|---|---|---|---|---|---|
| no. | Field | Saturated | Assumed | Beta[a] | Gamma | Total[b] | Total[c] |
| 2778 | 8.2 | 13.0 | 12 ± 2 | 1.06 ± 0.07 | 0.55 ± 0.02 | 1.73 ± 0.07 | 1.71 ± 0.07 |
| 2779 | 7.6 | 12.0 | 11 ± 2 | 0.93 ± 0.07 | 0.45 ± 0.02 | 1.49 ± 0.05 | 1.51 ± 0.05 |
| 2780 | 5.5 | 12.9 | 13 ± 4 | 0.92 ± 0.07 | 0.46 ± 0.03 | 1.49 ± 0.06 | 1.49 ± 0.06 |
| 2781 | 3.9 | 14.6 | 12 ± 5 | 0.93 ± 0.07 | 0.43 ± 0.03 | 1.48 ± 0.07 | - |
| 2782 | 4.4 | 15.1 | 13 ± 5 | 0.89 ± 0.08 | 0.44 ± 0.03 | 1.44 ± 0.07 | - |
| 2783 | 3.1 | 16.7 | 14 ± 7 | 0.90 ± 0.08 | 0.42 ± 0.03 | 1.43 ± 0.08 | 1.43 ± 0.08 |
| 2784 | 3.6 | 20.6 | 12 ± 8 | 0.84 ± 0.10 | 0.42 ± 0.04 | 1.38 ± 0.10 | 1.38 ± 0.10 |
| 2785 | 3.2 | 13.6 | 14 ± 5 | 0.82 ± 0.07 | 0.42 ± 0.03 | 1.35 ± 0.08 | 1.35 ± 0.08 |

Table 3-3: Water contents, and effective beta and gamma dose rates following water correction.

[a] Effective beta dose rate combining water content corrections with inverse grain size attenuation factors obtained by weighting the 200 μm attenuation factors of Mejdahl (1979) for K, U, and Th by the relative beta dose contributions for each source determined by Gamma Spectrometry.

[b] includes a cosmic dose contribution

[c] with a reconciliation of the effective gamma dose rate as determined below

| SUTL no. | depth / cm | distance from dating sample / r | weighting factor / $e^{-\mu r}$ | gamma dose rate at each sampling position | gamma dose rate / mGy $a^{-1}$ |
|---|---|---|---|---|---|
| **2778** | **141** | **0** | **1.0** | 0.55 ± 0.02 | **0.54 ± 0.01** |
| 2779 | 156 | 15 | 0.233 | 0.45 ± 0.02 | - |
| 2780 | 176 | 35 | 0.030 | 0.47 ± 0.03 | - |
| 2778 | 141 | 15 | 0.233 | 0.55 ± 0.02 | - |
| **2779** | **156** | **0** | **1.0** | 0.45 ± 0.02 | **0.46 ± 0.01** |
| 2780 | 176 | 20 | 0.135 | 0.47 ± 0.03 | - |
| 2778 | 141 | 35 | 0.030 | 0.55 ± 0.02 | - |
| 2779 | 156 | 20 | 0.135 | 0.45 ± 0.02 | - |
| **2780** | **176** | **0** | **1.0** | 0.47 ± 0.03 | **0.46 ± 0.01** |
| **2783** | **143** | **0** | **1.0** | 0.42 ± 0.03 | **0.42 ± 0.01** |
| 2784 | 163 | 20 | 0.135 | 0.42 ± 0.04 | - |
| 2785 | 183 | 40 | 0.018 | 0.45 ± 0.03 | - |
| 2783 | 143 | 20 | 0.135 | 0.42 ± 0.03 | - |
| **2784** | **163** | **0** | **1.0** | 0.42 ± 0.04 | **0.42 ± 0.01** |
| 2785 | 183 | 20 | 0.135 | 0.45 ± 0.03 | - |
| 2783 | 143 | 40 | 0.18 | 0.42 ± 0.03 | - |
| 2784 | 163 | 20 | 0.135 | 0.42 ± 0.04 | - |
| **2785** | **183** | **0** | **1.0** | 0.45 ± 0.03 | **0.42 ± 0.01** |

Table 3-4: Weighting factors (μ=0.1), gamma dose rates at each position, and the calculated weighted mean gamma dose rates received at each of the sampling positions (in bold)

### 3.3.2. **Single aliquot equivalent dose determinations**

For equivalent dose determination, data from single aliquot regenerative dose measurements were analysed using the Risø TL/OSL Viewer programme to export integrated summary files that were analysed in MS Excel and SigmaPlot. Composite dose response curves were constructed from selected discs and for each of the eight preheating groups from each sample, and used to estimate equivalent dose values for each individual disc and their combined sets. Dose response curves for each of the eight preheating temperature groups and the combined data were determined using a fit to exponential function (Appendix B). There was no evidence of significant differences in normalised OSL ratios (both in natural and regenerated dose points) between subsets of discs pre-heated at temperatures from 200°C to 280°C). Accordingly composite dose response curves from selected discs for each sample were constructed and used to estimate equivalent dose values for each individual discs and their combined sets.

Single aliquots were rejected from further analysis based on the test dose sensitivity check, SAR criteria checks, the robust mean, feldspar contamination and radial plots. Table 3-5 summarises the quality evaluation checks on the SAR data (once filtered); the mean sensitivity of each aliquot and sensitivity change, the recycling ratio and zero dose response. Recycling ratios were within error of unity ranging between 0.97 ± 0.03 and 1.01 ± 0.02 across the sample set. Zero dose values were very slightly inflated, indicating some recuperation of signal during the SAR sequence, or incomplete bleaching within a single SAR cycle; however, at <1% of the normalised natural signals these values were negligible. A positive sensitivity change,

varying between 3 and 8% per cycle was noted for each sample, but this is accounted for in the SAR procedure.

| SUTL No. | Sensitivity / counts $Gy^{-1}$ | Sensitivity change per cycle / % | Recycling Ratio | Zero Dose / Gy | IRSL response / % | Dose recovery ratio |
|---|---|---|---|---|---|---|
| 2778 | 526 ± 111 | 7.2 ± 2.0 | 1.01 ± 0.02 | -0.15 ± 0.15 | 4.0 ± 3.4 | 1.07 ± 0.03 |
| 2779 | 425 ± 84 | 7.5 ± 1.5 | 1.00 ± 0.02 | 0.04 ± 0.02 | 8.2 ± 3.7 | 1.04 ± 0.04 |
| 2780 | 615 ± 109 | 7.7 ± 1.5 | 1.00 ± 0.02 | 0.04 ± 0.01 | 6.3 ± 4.2 | 0.93 ± 0.04 |
| 2781 | 309 ± 53 | 3.1 ± 0.8 | 1.01 ± 0.02 | 0.08 ± 0.03 | 3.0 ± 1.5 | 1.00 ± 0.03 |
| 2782 | 323 ± 140 | 2.7 ± 0.9 | 1.00 ± 0.02 | 0.05 ± 0.02 | 6.2 ± 3.6 | 1.03 ± 0.06 |
| 2783 | 496 ± 82 | 6.5 ± 1.3 | 0.97 ± 0.03 | 0.07 ± 0.01 | 0.3 ± 2.3 | 0.93 ± 0.04 |
| 2784 | 481 ± 56 | 4.9 ± 1.1 | 0.97 ± 0.01 | 0.05 ± 0.03 | 3.5 ± 1.3 | 1.03 ± 0.03 |
| 2785 | 222 ± 29 | 8.1 ± 1.3 | 0.99 ± 0.02 | -0.02 ± 0.15 | 2.3 ± 1.9 | 1.04 ± 0.04 |

Table 3-5: SAR quality parameters. Standard errors given.

### 3.3.3. **Age determinations**

The total dose rate is determined from the sum of the equivalent beta and gamma dose rates, and the cosmic dose rate. Age estimates are determined by dividing the equivalent stored dose by the dose rate. Uncertainty on the age estimates is given by combination of the uncertainty on the dose rates and stored doses, with an additional 5% external error. Table 3-6 lists the total dose rate, stored dose and corresponding age of the sample.

| SUTL no. | Field no. | Dose rate / mGy $a^{-1}$ | Stored dose / Gy | Age / ka | Calendar years / yrs BC |
|---|---|---|---|---|---|
| 2778 | HD03-OSL1 | 1.71 ± 0.07 | 12.5 ± 0.1 | 7.28 ± 0.32 | 5260 ± 320 |
| 2779 | HD03-OSL2 | 1.51 ± 0.05 | 11.3 ± 0.2 | 7.51 ± 0.36 | 5500 ± 360 |
| 2780 | HD03-OSL3 | 1.49 ± 0.06 | 13.4 ± 0.3 | 8.96 ± 0.48 | 6950 ± 480 |
| 2781 | HD04-OSL1 | 1.48 ± 0.07 | 10.3 ± 0.1 | 6.97 ± 0.33 | 4950 ± 330 |
| 2782 | HD04-OSL2 | 1.44 ± 0.07 | 12.0 ± 0.3 | 8.34 ± 0.43 | 6320 ± 430 |
| 2783 | HD05-OSL1 | 1.43 ± 0.08 | 11.8 ± 0.4 | 8.24 ± 0.51 | 6220 ± 510 |
| 2784 | HD05-OSL2 | 1.38 ± 0.10 | 10.3 ± 0.2 | 7.48 ± 0.55 | 5470 ± 550 |
| 2785 | HD05-OSL3 | 1.35 ± 0.08 | 12.9 ± 0.2 | 9.58 ± 0.56 | 7570 ± 560 |

Table 3-6: Quartz SAR OSL age estimates. Standard errors given.

## 4. Discussion and conclusions

The quartz OSL ages reported here for the sediment stratigraphies at Hardisty-03, -04 and -05, together with those previously reported for Hardisty-01 and -02, provide a high-resolution chronological framework to explore the temporal and spatial distribution of artefacts across the site.

The sediment chronologies established for each profile are internally coherent, spanning at HD03 from 7.3 ± 0.3 ka (SUTL2778) to 9.0 ± 0.5 ka (SUTL2780), at HD04 from 7.0 ± 0.3 ka (SUTL2781) to 8.3 ± 0.4 ka (SUTL2782), and at HD05 from 8.3 ± 0.5 ka (SUTL2783) to 9.6 ± 0.6 ka (SUTL2785). In combination with the sediment chronologies derived for HD-01, which range between 7.8 ± 0.7 ka (SUTL2692) and 11.7 ± 0.5 ka (SUTL2694), and for HD-02 from 4.5 ± 0.2 ka (SUTL2695) to 8.7 ± 0.5 ka (SUTL2697; Table 4-1), the data attest to near synchronous deposition across the site, and with local knowledge, scope for further age modelling including the use of Bayesian methods to refine the TAQ and TPQ age limits.

| SUTL no. | Field no. | Age / ka | Calendar years / yrs BC |
|---|---|---|---|
| *Hardisty section HD-01* | | | |
| 2692 | HD01-OSL1 | 7.8 ± 0.7 | 5830 ± 670 |
| 2693 | HD01-OSL2 | 7.8 ± 0.4 | 5820 ± 350 |
| 2694 | HD01-OSL3 | 11.7 ± 0.5 | 9720 ± 520 |
| *Hardisty section HD-02* | | | |
| 2695 | HD02-OSL1 | 4.5 ± 0.2 | 2530 ± 210 |
| 2696 | HD02-OSL2 | 6.8 ± 0.3 | 4780 ± 300 |
| 2697 | HD02-OSL3 | 8.7 ± 0.5 | 6700 ± 480 |

Table 4-1: HD01 and HD02, Quartz SAR OSL age constraints

Furthermore, the luminescence field profiles (Fig. 4-1), in combination with the quartz SAR OSL ages, provide some measure of control on the Early and Middle Holocene (the latter 'post-occupation') site formation processes. In profiles HD01 and HD02, stratigraphically distinct IRSL and OSL signal intensities, may relate to post-deposition weathering histories. In both profiles, IRSL signal intensities initially increase down section, but in the lower part of the sequence the signal intensities decrease. However, with the blue OSL signal, the signal intensities increase down section. The lower part of the section contains buried soils in which the feldspar component is significantly weathered to clays. Since luminescence measurements were conducted on bulk samples using a portable OSL reader, it would imply that the drop in the IRSL signal is a response of a fall in the feldspar content of the samples. The blue OSL signal which includes a quartz contribution does not display a similar drop because quartz is much more resistant to weathering.

In contrast, the luminescence profiles through HD03 and HD04, reveal stratigraphically progressive luminescence signals, consistent with a normal-age depth progression, implying little re-working of sediment through the sedimentary column.

However, the luminescence profile of HD05 reveals more complexity throughout its depositional history, with notable maxima and local inversions in luminescence intensities with depth from 150 cm, potentially reflecting reworking and re-deposition of sediment within this sequence. It is notable that the youngest age obtained from this profile, is out of chronological sequence, and at 7.5 ± 0.6 ka (SUTL2784) may provide a minimum age constraint for this phase of reworking.

Figure 4-1 shows the tentative temporal correlations drawn between the sediment ages obtained from profiles HD-01 to HD-05 (the inset emphases the spatial distribution of the studied sections). It is evident that the deposition of the lower units, encompassing the artefact-bearing horizons, occurred within the Early Holocene, indicating occupation in this area in the prehistoric period. From a continental climate historical perspective it is highly significant that the OSL ages record aeolian deposition in the Early Holocene, substantially after the retreat of the Laurentide Ice Sheet, in the transitional period between deglaciation and the more arid conditions at the beginning of the Holocene. As such, the chronologies reported here are consistent with previous studies that document regional landscape instability and early aeolian activity in the region between 9500 and 6500 cal BC (Wolfe et al., 2002).

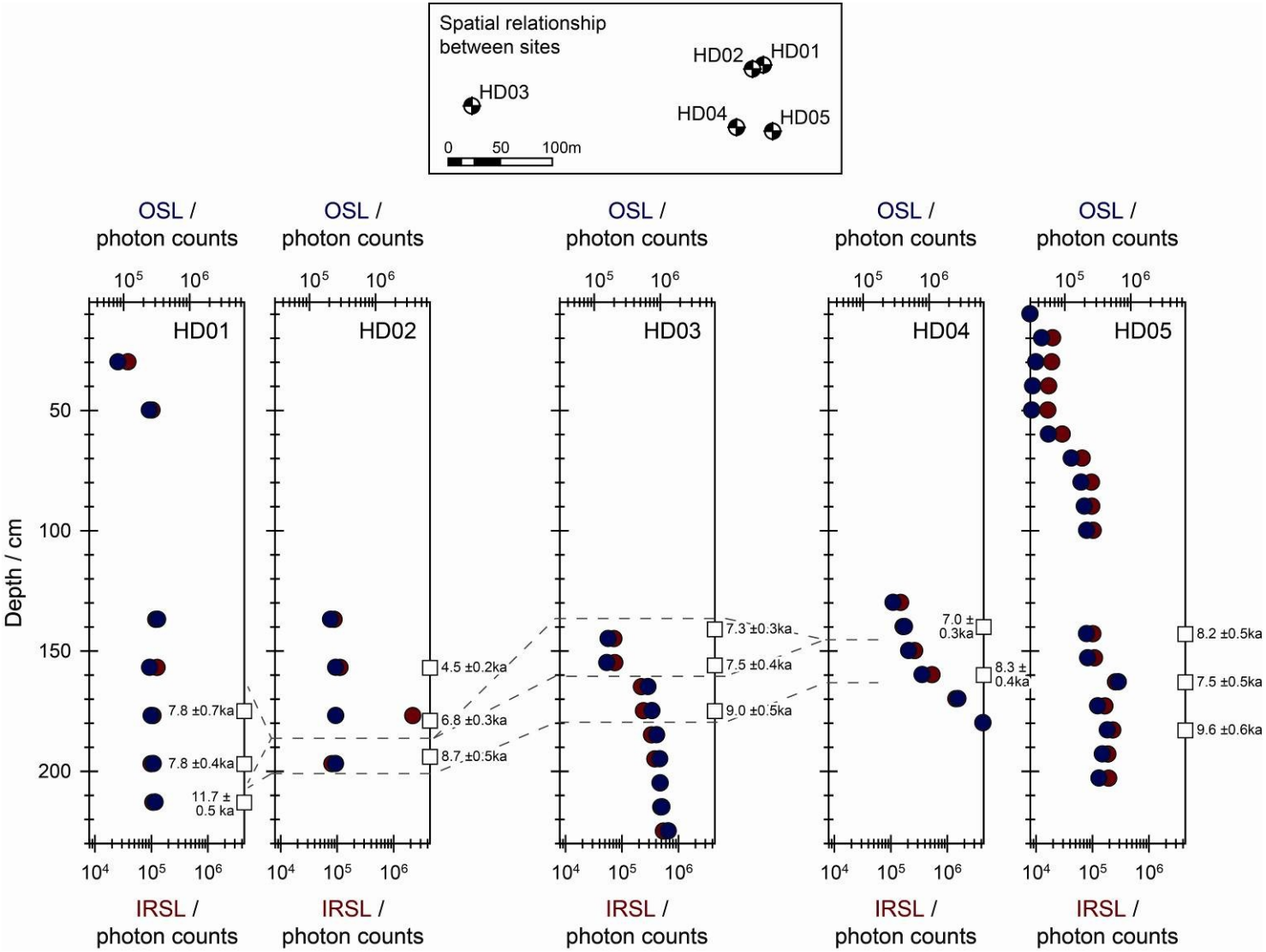


Figure 4-1: Temporal correlations between the sediment stratigraphies sampled at HD01 to HD05

The inset shows the spatial relationships between the different trenches

## 5. References


Aitken, M.J., 1983, Dose rate data in SI units: PACT, v. 9, p. 69–76.

Bøtter-Jensen, L., Bulur, E., Duller, G.A.T., and Murray, A.S., 2000, Advances in luminescence instrument systems: Radiation Measurements, v. 32, p. 523-528.

Kinnaird, T.C., Munyikwa, K., Sanderson, D.C.W., 2015, OSL investigations at Hardisty, Alberta, Canada. SUERC dating report. http://eprints.gla.ac.uk/110540/

Mejdahl, V., 1979, Thermoluminescence daing: Beta-dose attenuation in quartz grains Archaeometry, v. 21, p. 61-72.

Murray, A.S., and Wintle, A.G., 2000, Luminescence dating of quartz using an improved single-aliquot regenerative-dose protocol: Radiation Measurements, v. 32, p. 57-73.

NEA, 2000, The JEF-2.2 Nuclear Data Library: Nuclear Energy Agency, Organisation for economic Co-operation and Development. JEFF Report, v. 17.

Prescott, J.R., and Hutton, J.T., 1994, Cosmic ray contributions to dose rates for luminescence and ESR dating: Large depths and long-term time variations: Radiation Measurements, v. 23, p. 497-500.

Sanderson, D.C.W., 1987, Thermoluminescence dating of vitrified Scottish Forts: Paisley, Paisley college.

—, 1988, Thick source beta counting (TSBC): A rapid method for measuring beta dose-rates: International Journal of Radiation Applications and Instrumentation. Part D. Nuclear Tracks and Radiation Measurements, v. 14, p. 203-207.

Wolfe, S.A., Ollerhead, J., and Lian, O.B., 2002, Holocene Eolian Activity in South-central Saskatchewan and the Southern Canadian Prairies: Géographie physique et Quaternaire, v. 56, p. 215-227.

## Appendix A: Dose rate determinations, HD01 and HD02

| SUTL no. | Activity Concentration[a] / Bq kg$^{-1}$ | | | Equivalent Concentration[b] | | |
|---|---|---|---|---|---|---|
| | K | U | Th | K / % | U / ppm | Th / ppm |
| 2692 | 369 ± 16 | 7 ± 1.0 | 9 ± 1.0 | 1.19 ± 0.05 | 0.54 ± 0.07 | 2.32 ± 0.25 |
| 2693 | 382 ± 16 | 8 ± 1.0 | 14 ± 1.1 | 1.24 ± 0.05 | 0.66 ± 0.08 | 3.37 ± 0.26 |
| 2694 | 355 ± 15 | 10 ± 1.1 | 10 ± 1.0 | 1.15 ± 0.05 | 0.80 ± 0.09 | 2.53 ± 0.25 |
| 2695 | 361 ± 15 | 7 ± 0.9 | 11 ± 1.0 | 1.17 ± 0.05 | 0.60 ± 0.08 | 2.62 ± 0.25 |
| 2696 | 354 ± 16 | 8 ± 1.0 | 10 ± 1.0 | 1.14 ± 0.05 | 0.65 ± 0.08 | 2.46 ± 0.24 |
| 2697 | 395 ± 11 | 9 ± 0.5 | 13 ± 0.4 | 1.28 ± 0.03 | 0.70 ± 0.04 | 3.15 ± 0.10 |

Table A-1: Activity and equivalent concentrations of K, U and Th determined by HRGS

[a]Shap granite reference, working values determined by David Sanderson in 1986, based on HRGS relative to CANMET and NBL standards.

[b]Activity and equivalent concentrations for U, Th and K determined by HRGS (Conversion factors based on NEA (2000) decay constants): 40K: 309.3 Bq kg$^{-1}$ %K$^{-1}$, 238U: 12.35 Bq kg$^{-1}$ ppmU$^{-1}$, 232Th: 4.057 Bq kg$^{-1}$ ppm Th$^{-1}$.

| SUTL no. | HRGS, dry[a] / mGy a$^{-1}$ | | | TSBC, dry / mGy a$^{-1}$ |
|---|---|---|---|---|
| | Alpha | Beta | Gamma | |
| 2692 | 3.22 ± 0.28 | 1.14 ± 0.04 (3.9%) | 0.47 ± 0.02 (4.2%) | 1.22 ± 0.05 |
| 2693 | 4.33 ± 0.29 | 1.22 ± 0.05 (3.7%) | 0.55 ± 0.02 (3.7%) | 1.25 ± 0.05 |
| 2694 | 4.09 ± 0.30 | 1.14 ± 0.04 (3.8%) | 0.50 ± 0.02 (4.0%) | 1.01 ± 0.05 |
| 2695 | 3.61 ± 0.28 | 1.13 ± 0.04 (3.8%) | 0.49 ± 0.02 (4.0%) | 1.01 ± 0.04 |
| 2696 | 3.63 ± 0.28 | 1.11 ± 0.04 (4.0%) | 0.48 ± 0.02 (4.1%) | 1.27 ± 0.05 |
| 2697 | 4.26 ± 0.13 | 1.25 ± 0.03 (2.3%) | 0.55 ± 0.01 (2.0%) | 1.19 ± 0.05 |

Table A-2: Infinite matrix dose rates determined by HRGS and TSBC.

[a]based on dose rate conversion factors in Aikten (1983) and Sanderson (1987)

| SUTL no. | Water content / % | | | Effective Dose Rate / mGy a$^{-1}$ | | |
|---|---|---|---|---|---|---|
| | Fractional | Saturated | Assumed | Beta[a] | Gamma | Total[b] |
| 2692 | 20.4 | 21.1 | 20.6 ± 2 | 0.89 ± 0.05 | 0.38 ± 0.02 | 1.44 ± 0.06 |
| 2693 | 24.3 | 29.5 | 25.6 ± 3 | 0.88 ± 0.05 | 0.43 ± 0.02 | 1.48 ± 0.07 |
| 2694 | 26.4 | 28.5 | 27.0 ± 2 | 0.76 ± 0.05 | 0.38 ± 0.02 | 1.32 ± 0.06 |
| 2695 | 21.2 | 23.8 | 21.9 ± 2 | 0.79 ± 0.05 | 0.39 ± 0.02 | 1.36 ± 0.06 |
| 2696 | 21.3 | 21.5 | 21.3 ± 2 | 0.89 ± 0.05 | 0.39 ± 0.02 | 1.45 ± 0.06 |
| 2697 | 24.2 | 24.5 | 24.3 ± 2 | 0.89 ± 0.04 | 0.43 ± 0.01 | 1.49 ± 0.06 |

Table A-3: Water contents, and effective beta and gamma dose rates following water correction.

[a] Effective beta dose rate combining water content corrections with inverse grain size attenuation factors obtained by weighting the 200 μm attenuation factors of Mejdahl (1979) for K, U, and Th by the relative beta dose contributions for each source determined by Gamma Spectrometry.

[a] includes a cosmic dose contribution

**Appendix B: Dose Response Curves**

***Quartz Composite Dose Response Curves***

Figure B-1: Composite dose response curves for SUTL2778

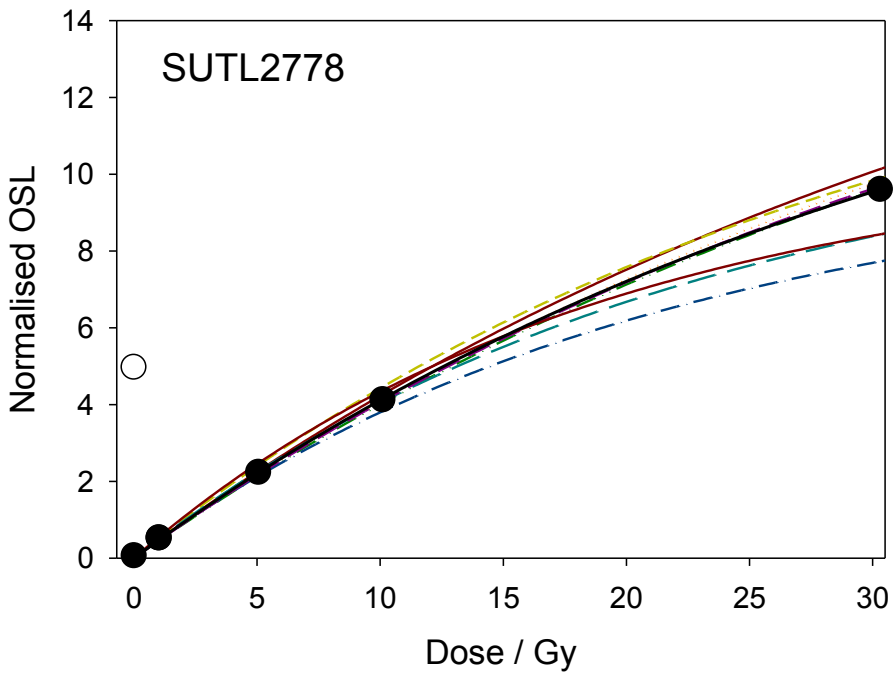


Lx = 1, 5, 10, 30, 0 and 1 Gy;
Tx = 2 Gy

Black line, All Preheats;
Coloured lines, specific preheats

Figure B-2: Composite dose response curves for SUTL2779

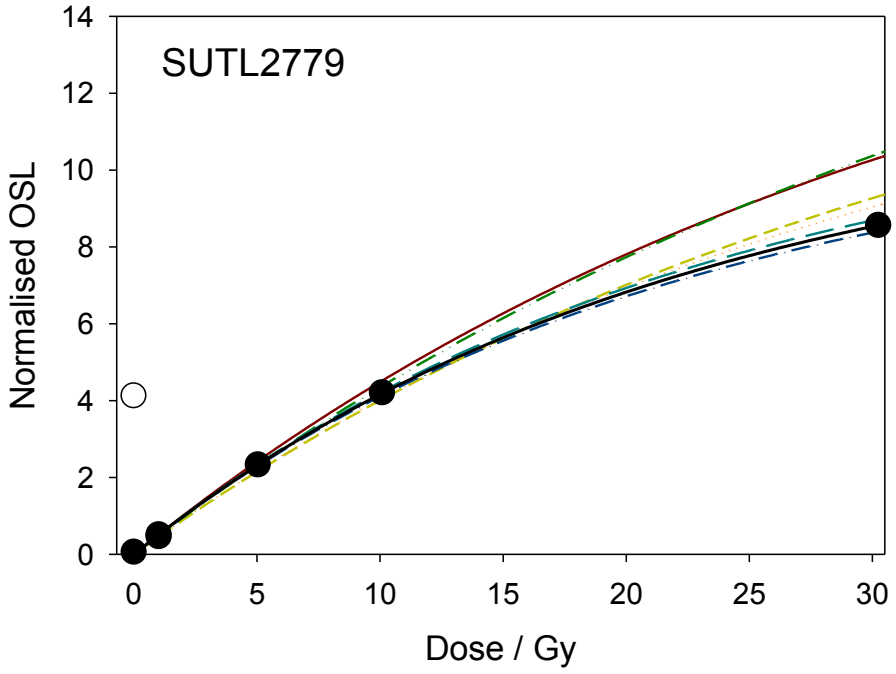


Lx = 1, 5, 10, 30, 0 and 1 Gy;
Tx = 2 Gy

Black line, All Preheats;
Coloured lines, specific preheats

Figure B-3: Composite dose response curves for SUTL2780

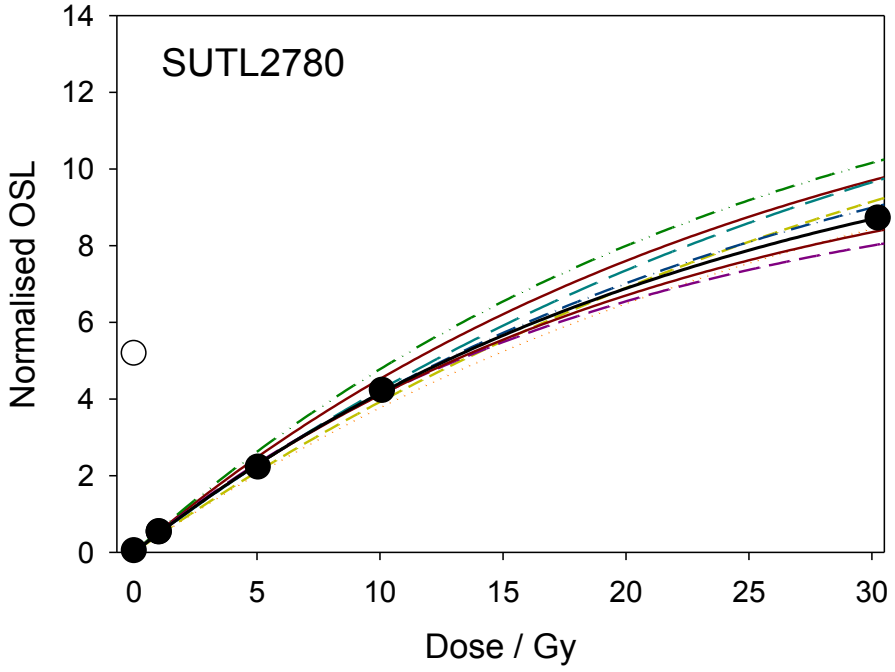


Lx = 1, 5, 10, 30, 0 and 1 Gy;
Tx = 2 Gy

Black line, All Preheats;
Coloured lines, specific preheats

Figure B-4: Composite dose response curves for SUTL2781

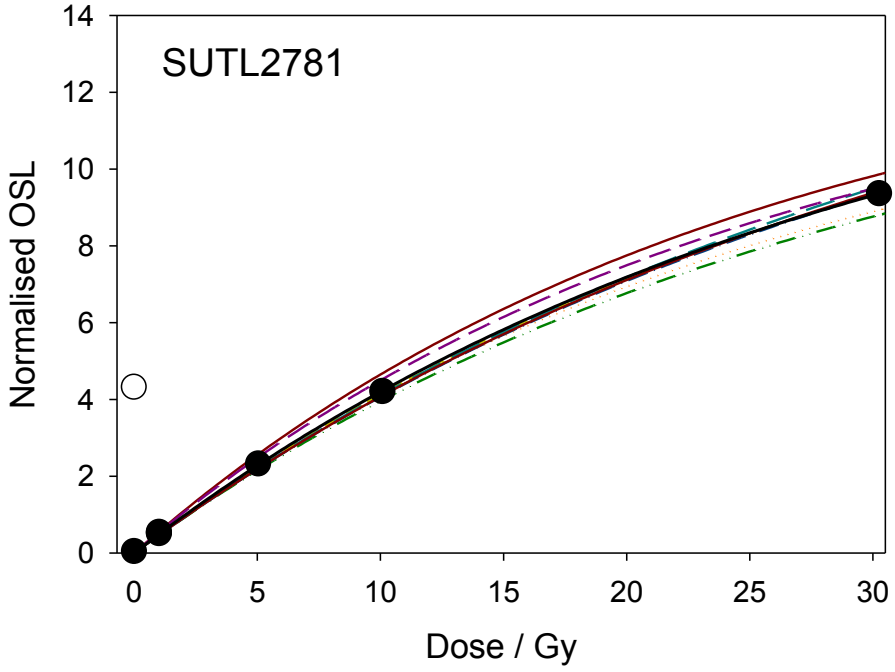


Lx = 1, 5, 10, 30, 0 and 1 Gy;
Tx = 2 Gy

Black line, All Preheats;
Coloured lines, specific preheats

Figure B-5: Composite dose response curves for SUTL2782

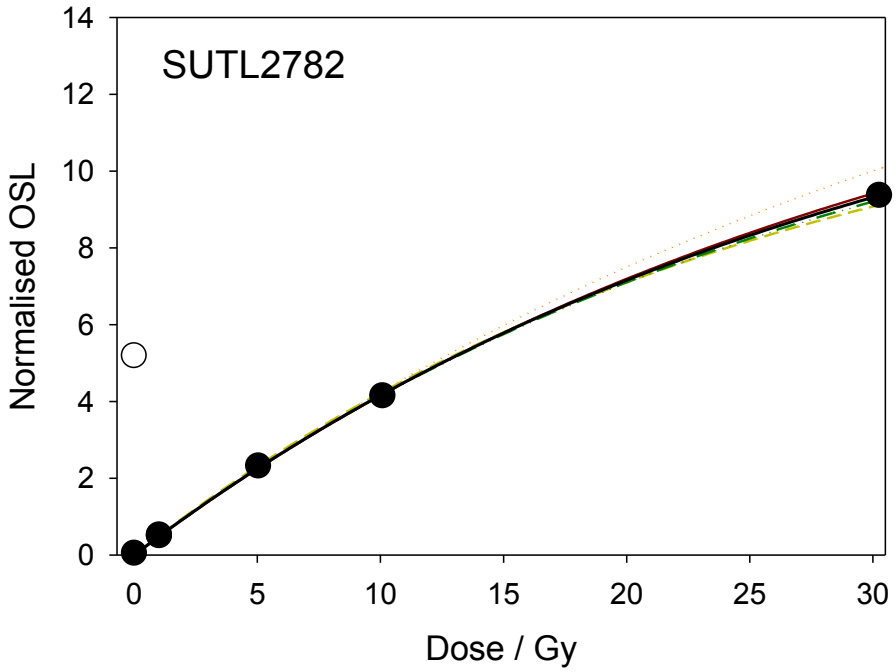


Lx = 1, 5, 10, 30, 0 and 1 Gy;
Tx = 2 Gy

Black line, All Preheats;
Coloured lines, specific preheats

Figure B-6: Composite dose response curves for SUTL2783

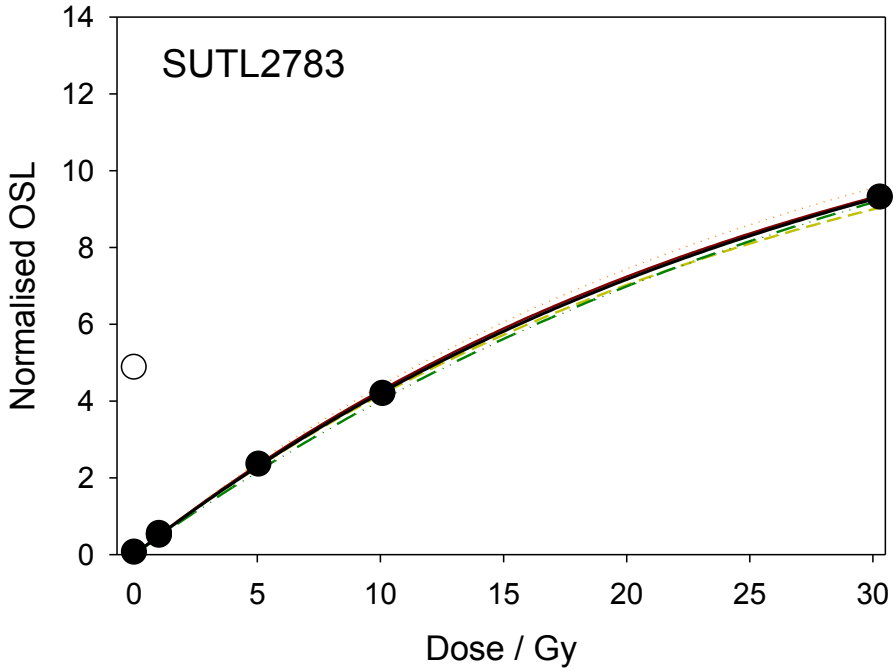


Lx = 1, 5, 10, 30, 0 and 1 Gy;
Tx = 2 Gy

Black line, All Preheats;
Coloured lines, specific preheats

Figure B-7: Composite dose response curves for SUTL2784

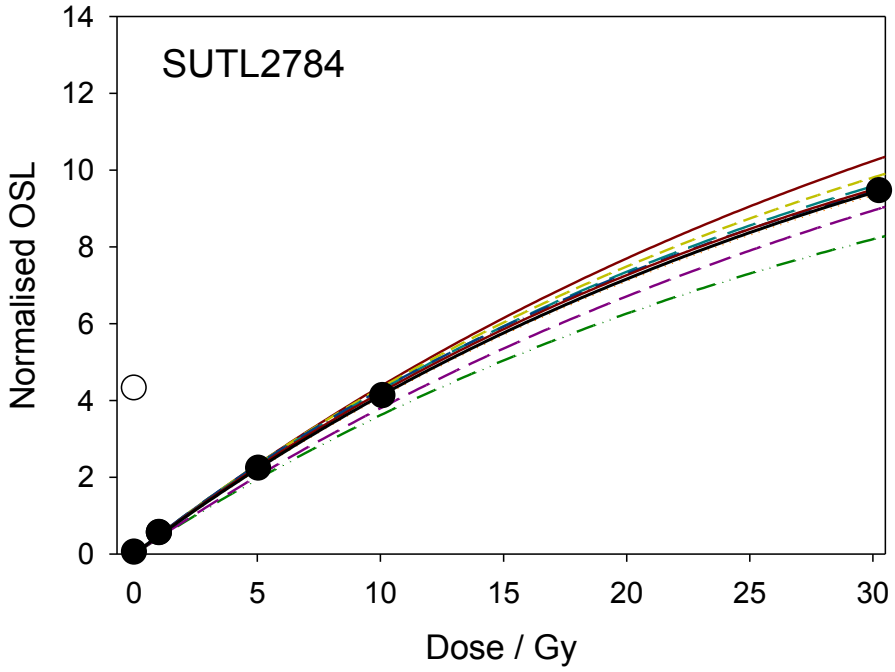


Lx = 1, 5, 10, 30, 0 and 1 Gy;
Tx = 2 Gy

Black line, All Preheats;
Coloured lines, specific preheats

Figure B-8: Composite dose response curves for SUTL2785

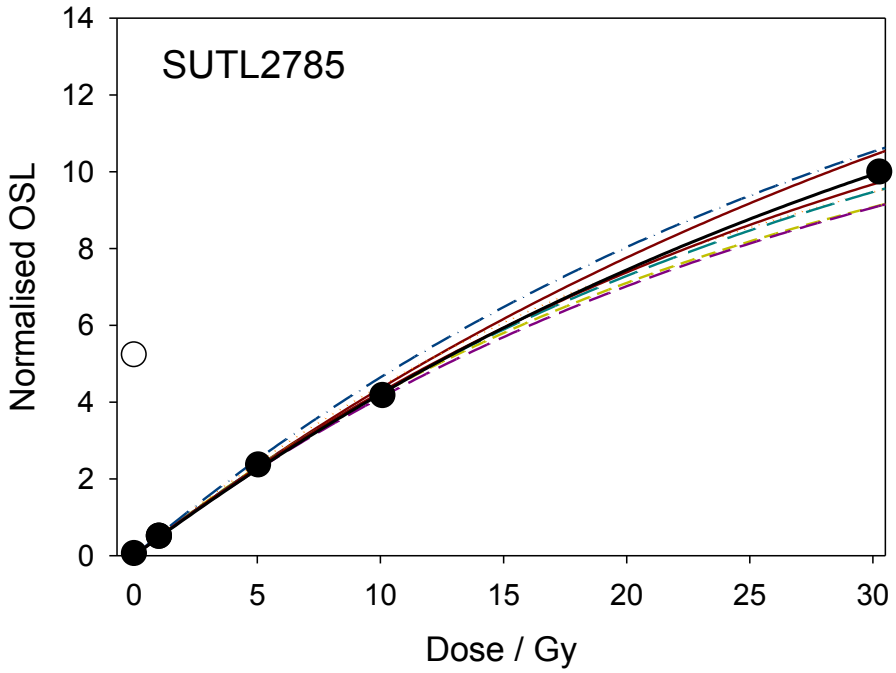


Lx = 1, 5, 10, 30, 0 and 1 Gy;
Tx = 2 Gy

Black line, All Preheats;
Coloured lines, specific preheats

## Appendix C: Abanico plots

Figure C-1: Abanico Plot for SUTL2778

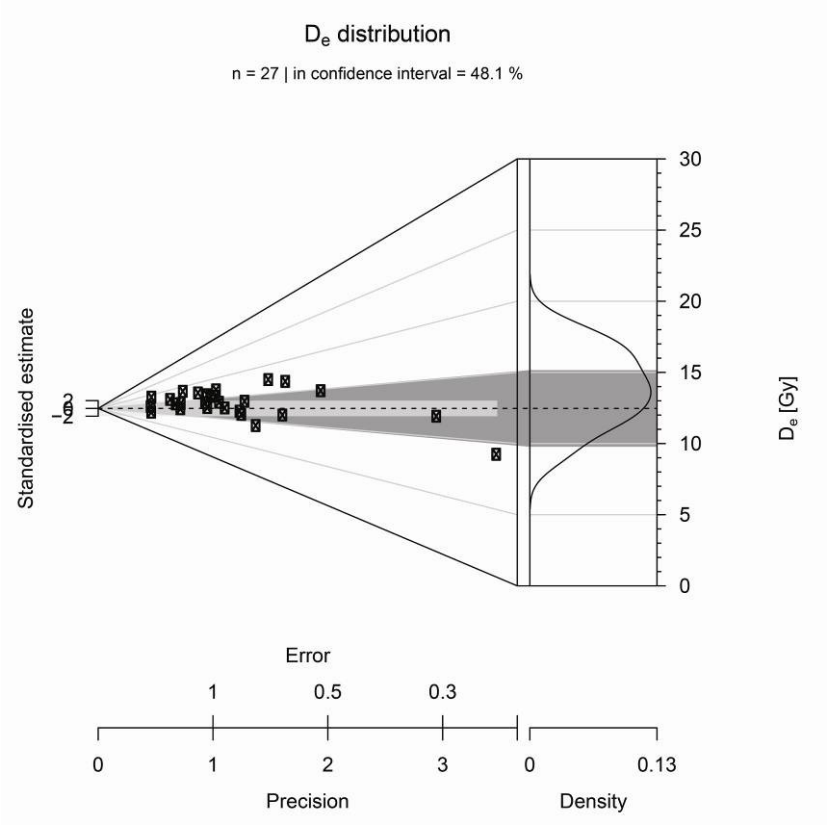


Figure C-2: Abanico Plot for SUTL2779

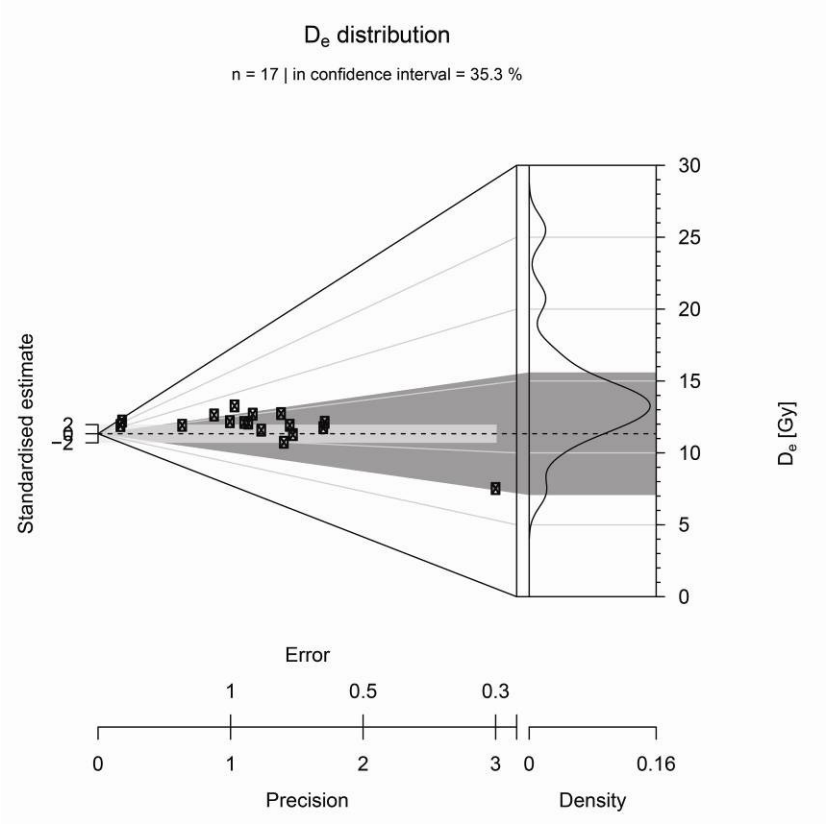

Figure C-3: Abanico Plot for SUTL2780

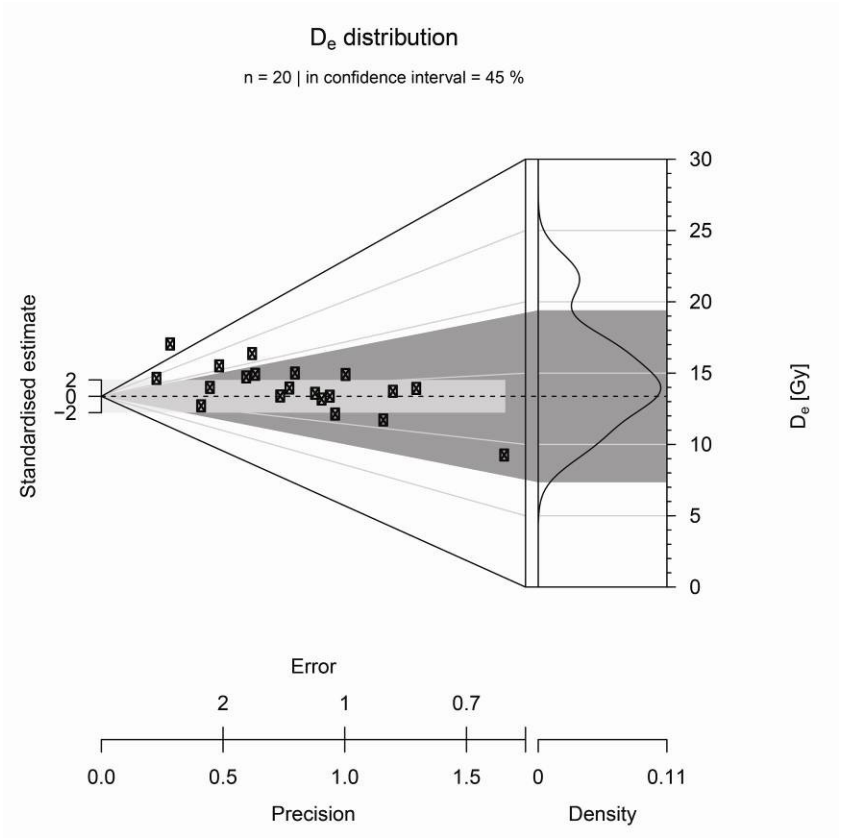


Figure C-4: Abanico Plot for SUTL2781

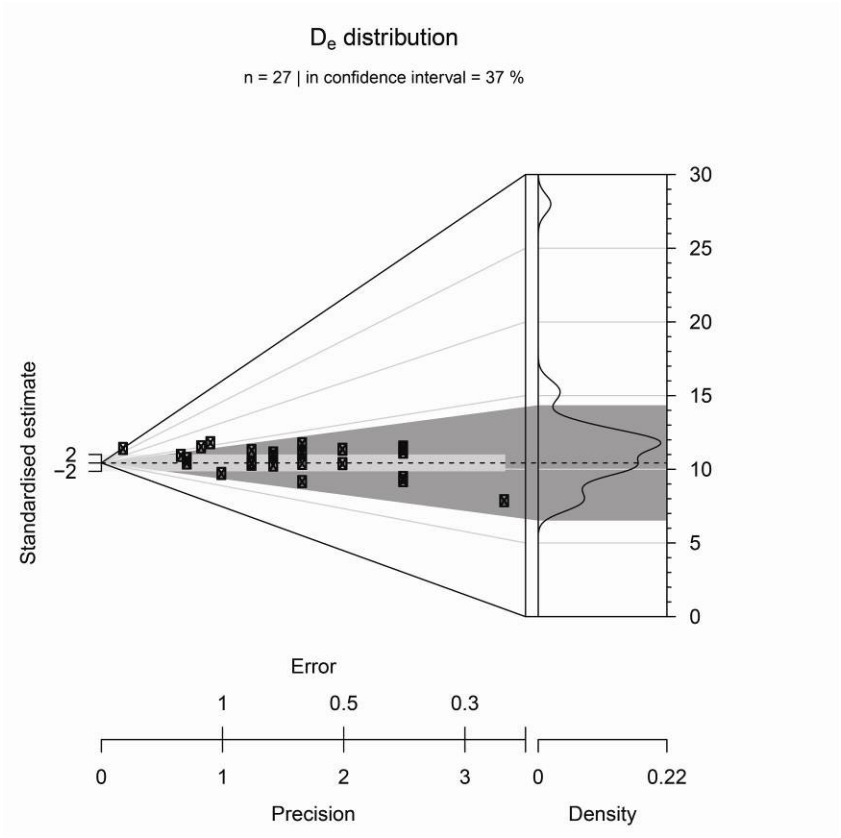

Figure C-5: Abanico Plot for SUTL2782

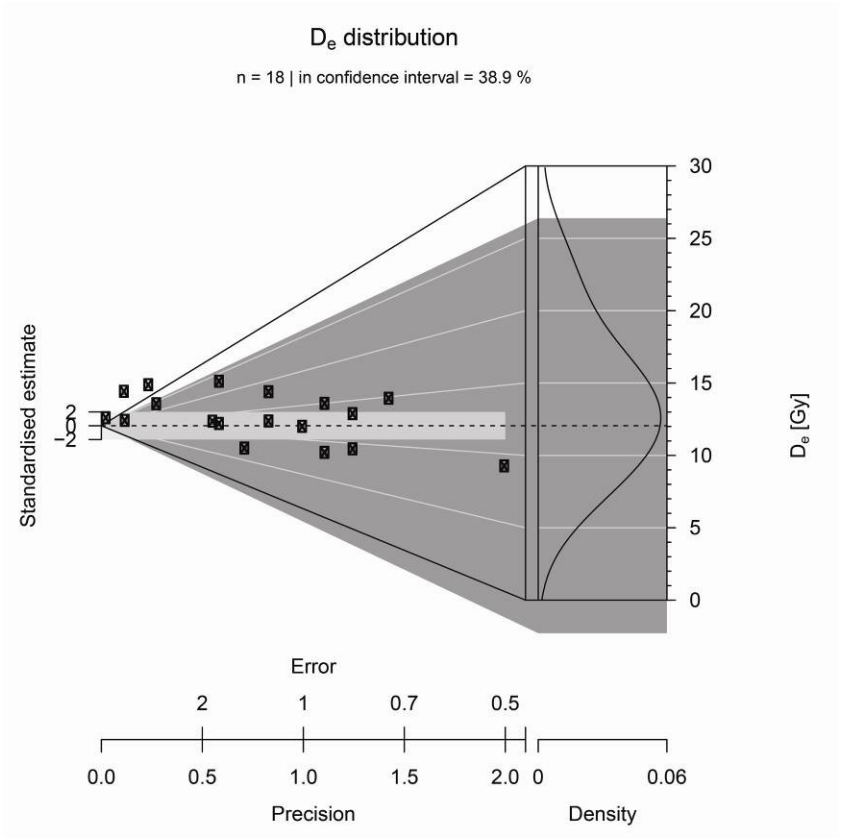


Figure C-6: Abanico Plot for SUTL2783

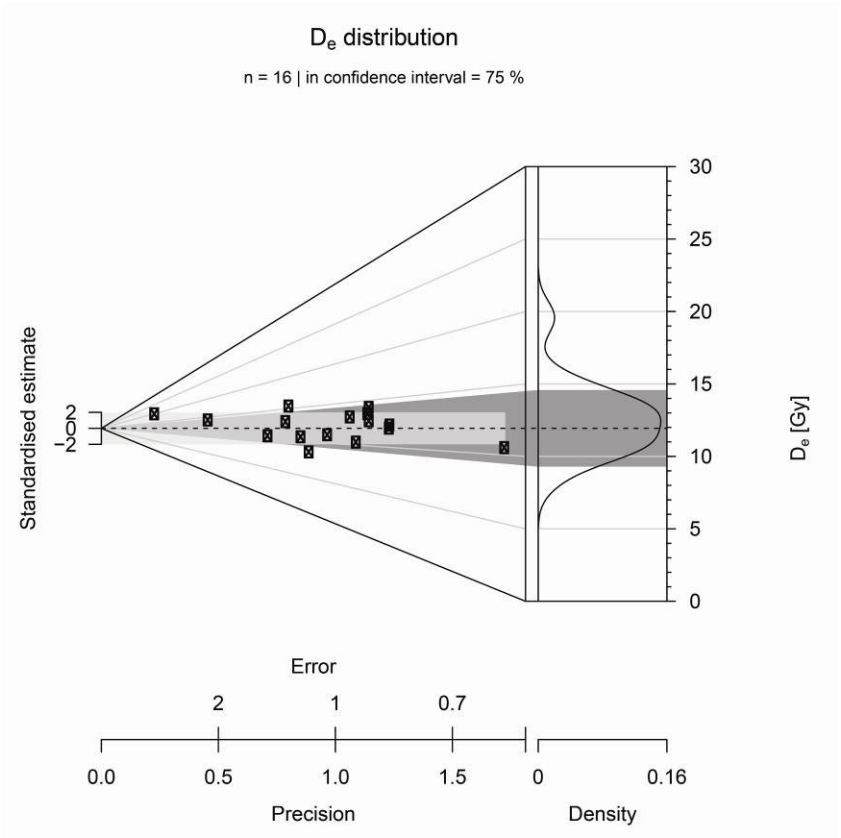

Figure C-7: Abanico Plot for SUTL2784

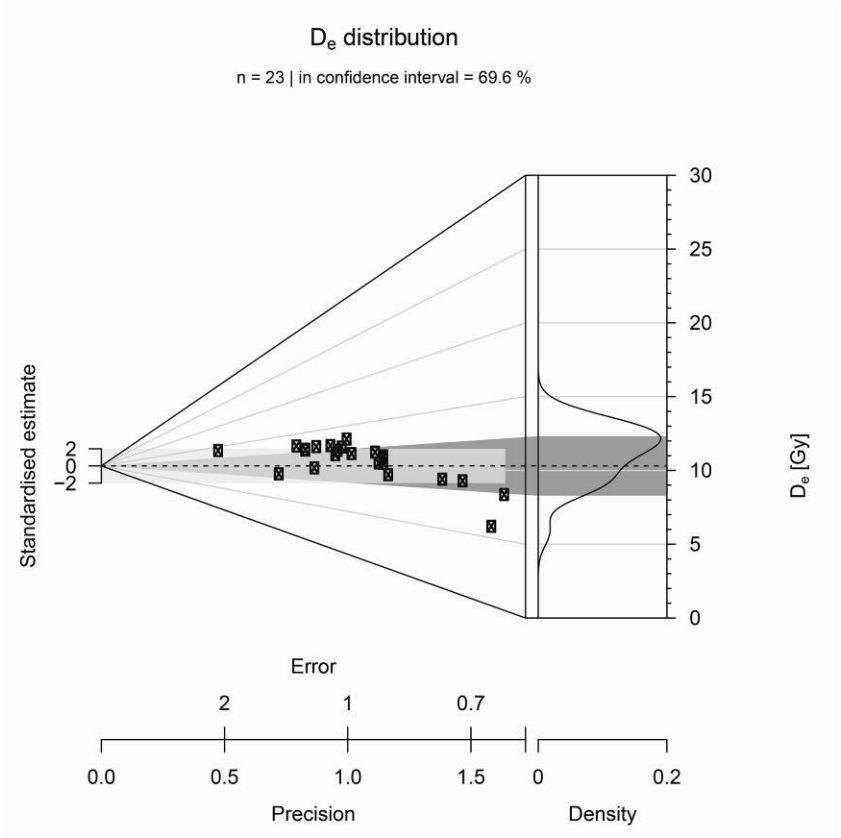


Figure C-8: Abanico Plot for SUTL2785